Nano Research

ISSN 1998-0124 CN 11-5974/O4
https://doi.org/10.1007/s12274-024-6586-5

Research Article

Improving the hydrostability of zeolitic imidazolate framework coatings using a facile silk fibroin protein modification method

Xiuming Wei[1], Ting Chen[1], Siyu Chen[1], Qian Jia[2], Nurul Ain Mazlan[1], Allana Lewis[1], Nobert Radacsi[1], and Yi Huang[1] (✉)

[1] School of Engineering, Institute for Materials & Processes, The University of Edinburgh, Robert Stevenson Road, Edinburgh, EH9 3FB, UK
[2] EASTCHEM School of Chemistry, The University of St Andrews, Purdie Building, North Haugh, St Andrews, KY16 9ST, UK

Received: 7 January 2024 / **Revised:** 23 February 2024 / **Accepted:** 25 February 2024

ABSTRACT

Zeolitic imidazolate frameworks (ZIFs) are an important subclass of metal-organic frameworks (MOFs) with zeolite-type topology, which can be fabricated under ambient synthesis conditions. However, the applications of ZIFs are commonly limited due to the weak hydrostability of their metal–ligand coordination bonds, particularly under humid and aqueous conditions. In this work, as an example, the hydrolysis behaviours of ZIF-L with a special focus on ZIF-L coatings were tested at aqueous conditions with a wide range of pHs to systematically study and fundamentally understand their structural stability and degradation mechanism. Pristine ZIF-L powder and ZIF-L coatings were severely damaged after only 24 h in aqueous media. Interestingly, the ZIF-L coatings showed two distinct hydrolyzation pathways regardless of pH conditions, exhibiting either a ring-shaped etching or unfolding behaviours. While the ZIF-L powders were hydrolyzed almost identically across all pH conditions. With this new understanding, a facile silk fibroin (SF) protein modification method was developed to enhance the hydrostability of ZIF-L coatings in aqueous media. The effect of protein concentration on surface coating was systemically studied. ZIF-L coating retained its surface morphology after soaking in water and demonstrated switchable super wetting properties and superior separation performance for oil/water mixture. As a result, the quick SF protein modification significantly enhanced the stability of ZIF-L coatings under various pHs, while retaining their switchable wetting property and excellent separation performance.

KEYWORDS

zeolitic imidazole framework-L (ZIF-L), ZIF-L coatings, silk fibroin protein, hydrostability enhancement, oil/water separation

1 Introduction

Metal-organic frameworks (MOFs), constructed by metal ions and organic linkers through coordination bonds, have enriched the family of porous materials. Due to their flexibility in forming functional structures with precise geometry, size, and functionality, MOFs with a crystalline nature generally possess high surface areas and tunable pore sizes [1]. Among the abundant existing MOFs, zeolitic imidazolate frameworks (ZIFs), constructed with tetrahedral metal ions and imidazolate-based organic ligands, have been extensively studied. ZIFs possess excellent structural tunability, simplicity, and cost-effectiveness in ambient-temperature synthesis and scale-up [2, 3]. These properties provide them great opportunities in a variety of applications, such as gas and liquid separations [4], catalysis [5], and drug delivery [6]. For example, the hierarchically nanostructured functional ZIF-L@SiC membranes exhibited high flux and synergistic features for iodine adsorption [7]. Using a two-step synthesis, ZIF-L coated three-dimensional (3D) printed membranes were fabricated with a hierarchically micro/nanoscale structural surface, which showed a high oil rejection of over 99% and flux of over 24,000 $L \cdot m^{-2} \cdot h^{-1}$ [8]. From the structural stability point of view, low-valent metal ions, such as Zn^{2+} and Co^{2+}, are normally considered as soft acids to construct highly stable MOFs with suitable N-containing linkers, such as ZIFs. The high pKa of azoles and the strong coordination bonds usually endow these MOFs with remarkable stability in the basic environment [9]. For example, the powder X-ray diffraction (PXRD) pattern of ZIF-8 remained unchanged after 3 days in a pH = 12 solution, and only a slight reduction in the Langmuir surface area was noted [10]. Furthermore, ZIF-8 retained its structure in boiling water for 7 days and its PXRD pattern remained unchanged up to 24 h in 0.1 and 8 M aqueous sodium hydroxide at 100 °C [11]. However, the application of ZIFs was limited due to the weak stability of the metal–ligand coordination (Zn–N) bond under acidic conditions regardless of the satisfactory performance of ZIF [12, 13]. For example, the ZIF-8 structures were immediately dissolved in a concentrated HCl solution [10]. In our previous study, the ZIF-L coated stainless steel mesh demonstrated hierarchical ZIF-L coating with unique switchable wetting properties and showed satisfactory oil/water separation performance of 99% removal efficiency [14]. However, the meshes suffered from weak stability in pH = 4 HCl solution and most ZIF-L coating was severely damaged after 6 h.

In recent years, a large number of strategies for improving the stability of existing MOFs have been developed, such as organic linker functionalization, post-synthetic modification, surface hydrophobic treatment, and hybridization of MOFs and

Address correspondence to Yi.Huang@ed.ac.uk

hydrophobic additives [9, 15, 16]. For example, the incorporation of poly-L-glutamic acid in ZIF-L has significantly enhanced the stability in mild acidic solutions [17]. Liu et al. reported that the hydrothermal stability of ZIF-8 could be remarkably improved via a shell ligand exchange reaction when using the functionalized 5,6-dimethyl benzimidazole as the ligands, owing to its hydrophobicity and steric hindrance effect [18]. As mentioned earlier, the excellent compatibility of MOFs with other materials allows the fabrication of a large number of attractive composite materials [19, 20]. For example, multi-wall carbon nanotubes can be incorporated into MOF-5 structures to achieve a composite material with a greater Langmuir-specific surface, significantly increasing H_2 storage capacity and stability in the presence of moisture [21]. Moreover, Zhang et al. developed a facile and general polydimethylsiloxane (PDMS) coating strategy to enhance the stability of MOFs in the presence of moisture or water [22]. As a result, the hydrostability of MOF-5, HKUST-1, and ZnBT was significantly enhanced via PDMS coating owing to the change in the surface wettability. The above studies demonstrated enhanced hydrostability of MOF but inevitably altered the surface wettability, which could inhibit some interesting properties such as the switchable wettability of MOF-coated materials. Moreover, there are very limited studies focusing on the understanding of the hydro-stability of supported MOF/ZIF coatings which have far more complicated crystal packing and intergrowth than powdered samples. Likely, MOF-coated materials behave very differently when contacting water. Therefore, it is of practical importance to directly study their hydrostability under harsh aqueous conditions.

Herein, we report a facile method of improving the hydrostability of ZIFs (taking ZIF-L as an example as it is less thermodynamically stable than most ZIF materials) by simply coating a layer of silk fibroin (SF) protein without altering its original surface wetting property. Silk fibroin protein has been widely studied due to its unique combination of biocompatible, structural, and robust mechanical properties [23, 24]. Fibroin molecules act as hydrophilic–hydrophobic–hydrophilic polymers and form micelles in water through chain folding and hydrophobic interactions, with hydrophilic blocks on the outside and hydrophobic tails on the inside [25]. The hydrolysis behaviour of pristine ZIF-L coated stainless steel (ZIF-L-SS) meshes under different pHs was studied. In the meantime, the hydrolysis of ZIF-L powders under different pHs was also monitored accordingly to understand and compare their hydrolyzation process. The effects of SF protein concentration on coating formation were systematically studied. According to our results, the changes of hierarchical morphology and switchable wettability of ZIF-L coated meshes were found crucial importance in the oil/water separation performance, therefore, they were carefully monitored throughout the hydrostability tests. Notably, the SF-modified ZIF-L stainless steel mesh (SF-ZIF-L-SS) exhibited outstanding performance in oil/water separation even after the hydrostability tests.

2 Experimental

2.1 Materials

Zinc nitrate hexahydrate ($Zn(NO_3)_2{\cdot}6H_2O$; 98%), 2-methylimidazole (Hmim; 99%), and lithium bromide (LiBr, 99%) were purchased from Sigma-Aldrich Company Ltd. Stainless steel meshes (400 mesh/77 μm) were purchased from the Mesh Company (Warrington) Ltd. Silk cocoons were purchased from Wild Fibers Ltd. UK. Methanol (98%), chloroform (99%), and hexane (99%) were supplied by Fisher Scientific UK Ltd.

2.2 Preparation of ZIF-L-SS mesh and powder

Stainless steel mesh was cut into the size of 2 cm × 4 cm and was sequentially washed in acetone, ethanol, and hydrochloric acid to remove surface impurities. The ZIF-L mesh was synthesized according to the literature following a pre-seeding and secondary growth process [14]. 0.59 g of $Zn(NO_3)_2{\cdot}6H_2O$ and 1.31 g of Hmim were dissolved in 50 mL of deionized (DI) water, respectively, and then mixed to complete the ZIF-L seed synthesis solution. One piece of stainless-steel mesh was placed vertically in the synthesis solution and stirred at 25 °C for 20 min. After that, the seeded mesh was vertically immersed in the freshly prepared synthesis solution for secondary growth. After 1 h, the mesh was removed and washed with deionized water. Then the mesh was dried in the oven at 60 °C for 12 h. ZIF-L powder was collected from the same synthesis solution after 24 h, washed with methanol, and dried in the oven at 60 °C for 12 h.

2.3 Preparation of SF-ZIF-L-SS mesh and powder

The silk fibroin protein stock solution was fabricated by a chemical degummed method [24]. Briefly, Bombyx mori cocoons were boiled for 30 min in an aqueous solution of 0.02 M sodium carbonate and then rinsed thoroughly with deionized water to remove the glue-like sericin. After air drying, the extracted silk fibroin was dissolved in 9.3 M LiBr solution at 60 °C for 4 h. The solution was dialyzed against distilled water using a dialysis tube (MWCO 3500, Pierce) for 72 h to remove the salt. The solution was then centrifuged twice at 10,000 rpm for 15 min to remove sediments which were silk aggregates and debris from original cocoons. The final concentration of silk fibroin aqueous solution was approximately 3.9 wt.%, based on weighing the residual solid of a known volume of solution after drying at 60 °C. The silk stock solution was stored at 4 °C and diluted with deionized water before use.

The ZIF-L meshes were first vertically placed in the silk fibroin protein solution of different concentrations (0.5 wt.%, 1 wt.%, and 3 wt.%), and the coating solution was gently stirred at 200 rpm. Then the protein-coated meshes were taken out after 1 h and dried in the oven at 60 °C for 1 h. SF-ZIF-L powder (SF-ZIF-L-P) was prepared by stirring ZIF-L powder in 1% silk fibroin protein solution for 1 h, collected by centrifuge, and then dried in the oven at 60 °C for 12 h.

2.4 ZIF-L-SS mesh and powder hydrostability test

The stability tests were conducted by soaking the ZIF-L-SS and SF-ZIF-L-SS meshes coated with different concentrations of silk fibroin protein (0.5 wt.%, 1 wt.%, and 3 wt.%) in pH = 3 HCl solution, pH = 11 NaOH solution, and DI water (pH was adjusted by hydrochloride solution (1 M) and sodium hydroxide solution (1 M) because Cl^- and Na^+ were proved not to affect the structure of ZIF crystals [26]). Samples of the meshes were taken at various time points from 3 h to 7 days.

2.5 Oil/water separation

The oil/water separation performance of the meshes was tested by a gravity-driven oil/water mixture separation apparatus. Oil/water mixtures were prepared by simply mixing water with the oil(s). Methylene blue and oil red O were used to dye water and oil respectively for a clear visual observation. The mesh was placed between two identical glass tubes and then sealed firmly with clamps. In each separation test, the oil/water mixture was poured directly into the upper tube, then the permeate was collected with a beaker underneath, and the flux was monitored at the same time.

In a switchable oil/water separation test, the mesh was firstly

pre-wetted with water by carefully pouring ~ 20 mL of DI water onto the mesh surface. Then a mixture of water and cyclohexane was poured into the top funnel, and the permeated water was collected in a beaker. After that, the mesh was gently washed with ethanol and kept soaking for 10 min, followed by air drying for 5 min. The cleaned mesh was then fixed in the separation apparatus and pre-wetted with oil by pouring ~ 50 mL of dichloromethane onto the mesh surface. A mixture of chloroform and water was then poured into the top funnel, and the permeated dichloromethane was collected.

The permeate flux (F) of the mesh was calculated from the volume of the permeation in unit time according to Eq. (1)

$$F = V/(A \times t) \quad (1)$$

where V is the volume of the filtrate (L), A is the effective filtration area of the mesh (m^2), and t is the permeation time (h).

The separation efficiency (R%) was calculated using Eq. (2)

$$R\% = (1 - C_p/C_0) \times 100\% \quad (2)$$

where C_p is the residual oil concentration in the collected filtrate, and C_0 is the original oil concentration in the feed oil/water mixture.

2.6 Characterizations

The morphology change of the ZIF-L meshes was characterized by using a JEOS JSM-IT100 scanning electron microscopy (SEM). The crystalline structure of the synthesized ZIF-L was determined by X-ray diffraction (XRD, Bruker D8 Advance) with Cu Kα radiation in a 2θ range of 5.0°–40.0°. pH was measured by ETI 8000 pH meter. Contact angle (CA) measurements were performed on the Ossila Contact Angle Goniometer. Fourier transform infrared (FTIR) was characterized by Thermo Scientific Nicolet iS10 at the wavenumber of 4000–400 cm^{-1}. Nitrogen adsorption was measured by Quantachrome Autosorb IQ surface area analyzer in a nitrogen environment at 77 K. The powdered samples were initially degassed at 120 °C for 12 h to remove the weakly adsorbed moisture or guest molecules. The surface area and adsorption/desorption behaviour of the powdered samples were studied with the Brunauer–Emmett–Teller (BET) model. The total pore volume, V_{total}, was estimated from the desorption branch of the isotherm at P/P_0 = 0.99, assuming complete pore saturation. The residual oil content in the permeate solutions was characterized by a Shimadzu total organic carbon (TOC) analyser.

3 Results and discussion

3.1 Hydrostability of supported ZIF-L coatings and powder samples

Though the stability of ZIF materials was widely studied, most of the work focused on ZIF-8 and ZIF-67, and the stability of less thermodynamically stable ZIF-L was barely studied. In this work, the hydrostability of ZIF-L powder and coatings (ZIF-L-SS) was systematically studied under various aqueous solutions with different pHs.

3.1.1 Pristine ZIF-L-SS meshes

In this study, the soaked pristine ZIF-L-SS meshes were first characterized by SEM (Figs. 1(a)–1(g)) and XRD (Fig. 1(h)) to monitor the surface crystal morphological and structural changes. According to Figs. 1(a)–1(c), the pristine ZIF-L-SS mesh was uniformly covered with leaf-like ZIF-L crystals, where all ZIF-L crystals were densely and vertically packed on the mesh skeleton. Figures 1(d)–1(f) show that etchings on the ZIF-L crystal plane were more severe than the edge after 24 h in aqueous media regardless of the pH. However, the etching of the closely packed ZIF-L crystals in pH = 3 HCl solution was much faster than that in water (pH ≈ 7) and basic NaOH solution with a pH of 11 (Fig. S1 in Electronic Supplementary Material (ESM)). The *ab* plane of ZIF-L was severely damaged in pH = 3 HCl solution after 12 h (Fig. S1(a) in the ESM), leaving many ring-shaped residues on the mesh skeleton. While in water and basic solution, the crystals were only partially damaged (Figs. S1(c) and S1(e) in the ESM). After 24 h in pH = 3 solutions, the leaf-like morphology of the ZIF-L crystals was destroyed, indicating that most of the crystals were fully decomposed, leaving thin and stick-like residues on the mesh skeleton (Fig. S1(b) in the ESM). While in DI water and basic solution, all surface crystals showed a ring-shaped structure with most of the interior *ab* plane disappearing (Figs. S1(d) and S1(f) in the ESM). Note that a ZIF-L crystal model with *a*, *b*, and *c* coordinate axes is shown in Fig. 1(i). Similar ring etching has also been observed recently in other work for ZIF powder samples [27]. As reported, ring-like ZIF-8 crystals were formed after initial etching of the ZIF-L *ab* plane in an aqueous solution in the presence of $Zn(NO_3)_2$ and then a structural transformation of the outer ring to the more stable ZIF-8 phase. Similarly, in our work, the etching of ZIF-L crystals on the mesh surface commenced on the *ab* plane of the crystal, leaving a ring-shaped structure after 24 h. During the stability test, Zn^{2+} and Hmim from the decomposition of ZIF-L may provide nutrients to form a 3D ZIF on the edge, making it last longer in the aqueous environment [27].

Interestingly, a coexisting unfolding behaviour was also observed for a small portion of highly packed/intergrown ZIF-L crystals, forming a flower-like structure with stacks of thinner crystal sections (Fig. 1(g) and Figs. S2–S4 in the ESM). Compared to the previously mentioned *ab* plane etching process, the unfolding process and decomposition of the unfolded thin crystal sections were extremely slow. According to our study, most unfolded crystals retained their morphology over 15 days in both DI water and pH = 3 HCl solutions. In addition, these unfolded crystals presented an angled edge of a hexagon since day one (Figs. S2 and S3 in the ESM). In the pH = 11 solutions, the unfolded crystals showed a similar flower-like layered structure after 24 h, and then the crystals became thicker, shaper, and more elongated with the further increase of time (Fig. S4 in the ESM). The resemblance of ZIF-L coating dissolution under different pHs indicated that the etching process was similar in aqueous media regardless of the pH. It was then suggested that the dissolution started simultaneously in *a*, *b*, and *c* directions (where *a* and *b* were parallel to the ZIF-L crystal plane and *c* was vertical to the plane). Inside the ZIF-L structure, the two-dimensional (2D) structure along the *ab* plane is stacked along the *c* direction via the hydrogen bond of free ligand molecules [28], forming cushion-shaped cavities between layers with a dimension of the interlayer spacing of 9.4 Å × 7.0 Å × 5.3 Å which is larger compared to the pore size on *ab* plane/c direction (3.4 Å). The terminal Hmim ligand on the ZIF-L layer and "free" Hmim in between ZIF-L layers may have little hindrance effect, which makes it possible for water molecules to get in through the *a*/*b* direction [29, 30].

The co-existing ring-shaped etching and unfolding behaviours (Fig. 1(i)) might also be induced by steric hindrance formed by tight ZIF-L packing and intergrowth. As shown in Figs. 1(b) and 1(c), ZIF-L crystals were densely packed on the skeleton of the mesh, and some crystals were closely surrounded by others or even buried underneath. Therefore, water molecules only had limited access to all facets of these crystals. Thus, instead of etching through the *c* direction, water molecules could also only penetrate through the *b* direction because the crystals on the mesh skeleton

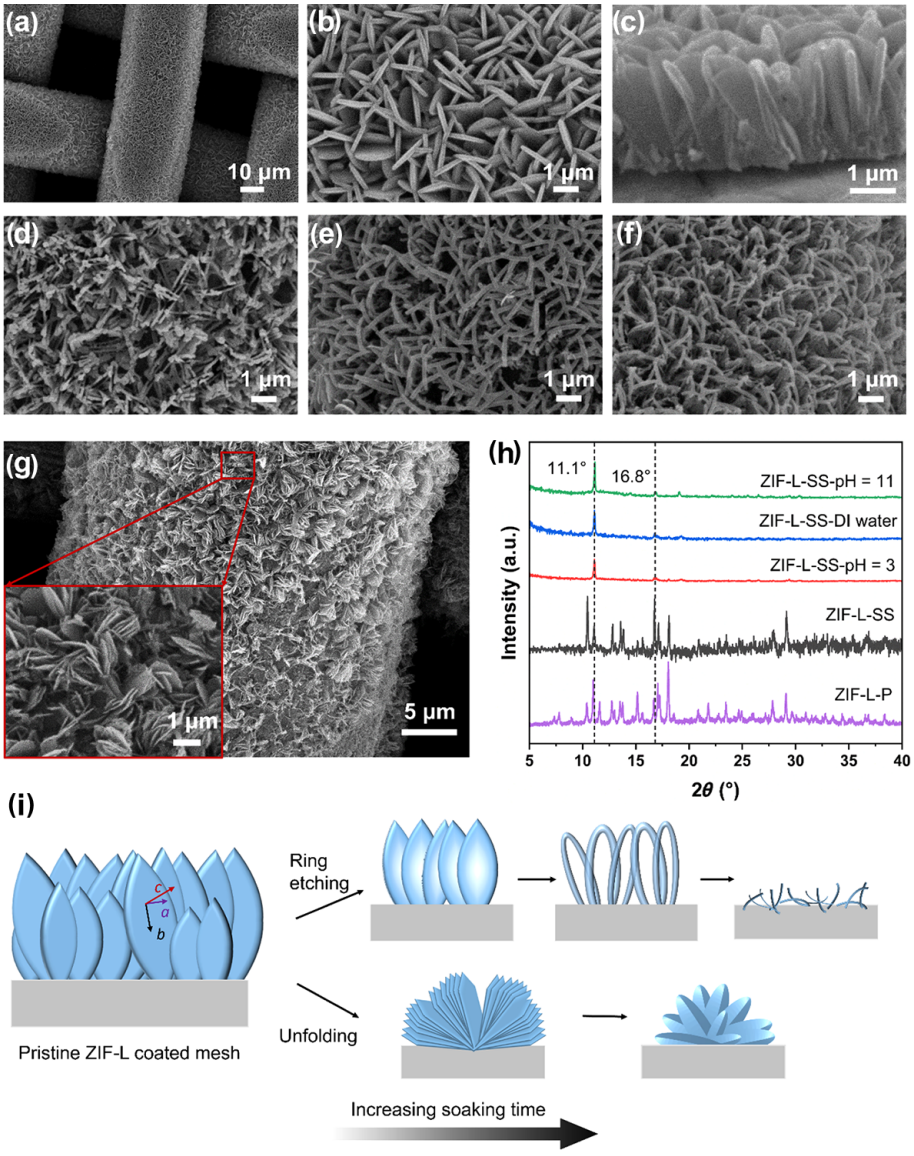

Figure 1 (a)–(c) SEM images of pristine ZIF-L coated mesh at different magnifications. (d)–(f) SEM images of ZIF-L mesh after being soaked in pH = 3 HCl solution, DI water, and pH = 11 NaOH solution for 24 h, respectively. (g) SEM images of ZIF-L-SS mesh after soaking in DI water for 24 h at different magnifications. (h) XRD patterns of original ZIF-L powder, ZIF-L-SS mesh, and ZIF-L-SS mesh after being soaked in pH = 3 HCl solution, DI water, and pH = 11 NaOH solution for 24 h. (i) Observed dissolution mechanisms for ZIF-L-SS meshes under acidic, neutral, and basic conditions.

were vertically oriented with the more exposed surface area on the *bc* plane for preferential water contact. On the other hand, restricted water contact on the *ab* plane of the crystals occurs due to the close packing of vertically aligned ZIF-L crystals. Eventually, after water contact, the ZIF-L crystals could be unfolded by breaking the hydrogen bond between adjacent layers. The angled edge on ZIF crystals was observed in pH = 3 HCl solution, DI water, and pH = 11 NaOH solution after 24 h. A similar edge-shape transition was reported by Lee et al., and the change in the edge shape was correlated with the additional growth of a 3D ZIF on the leaf-shaped crystal [27]. Zn^{2+} and imidazole from the decomposition of ZIF-L provide nutrients to form an aqueous stable zinc-containing compound, which could last longer in the water. In addition, such hexagonal nanoflake morphology of ZIF-L hydrolysis residue was commonly observed among zinc-containing compounds [31]. XRD patterns of pristine ZIF-L coated mesh and soaked mesh samples are shown in Fig. 1(h). The characteristic diffraction peaks of ZIF-L were observed on the ZIF-L-SS mesh after the seeded growth. However, after the stability test, most of the diffraction peaks from ZIF-L disappeared after 24 h except the peaks at 2θ = 11.1° (020) and 16.8° (101), indicating the severe damage to ZIF-L crystalline structure on the mesh skeleton. While the residue materials on the mesh were too low in quantity to get an XRD pattern, thus ZIF-L powders were tested at the same conditions and used for further characterizations and comparison.

3.1.2 *Pristine ZIF-L powders*

The SEM images of ZIF-L-P (ZIF-L powders) before and after hydrostability tests are shown in Figs. 2(a)–2(d), and interestingly, these fully hydrolyzed samples exhibited identical morphology with a cross shape regardless of pH value in the solutions (Fig. 2(e)), again indicating that pH was not the dominant contributor to the hydrolysis and the morphological change of ZIF-L in aqueous media.

As shown in Fig. 2(f), the FTIR spectra of the ZIF-L-P samples after 24 h stability test in aqueous media was still dominated by an intermediate ZIF-type structure. The highest absorption band at ~ 420 cm^{-1} corresponded to the Zn–N bond [32]. The other peaks between 410 and 540 cm^{-1} were attributed to the vibration of the Zn–O bond [32]. The signals in the spectral region of 900–1350 cm^{-1} were for the in-plane bending of the ring while those below 800 cm^{-1} were assigned as out-of-plane bending [33]. The peaks that were associated with the vibration of imidazole rings were

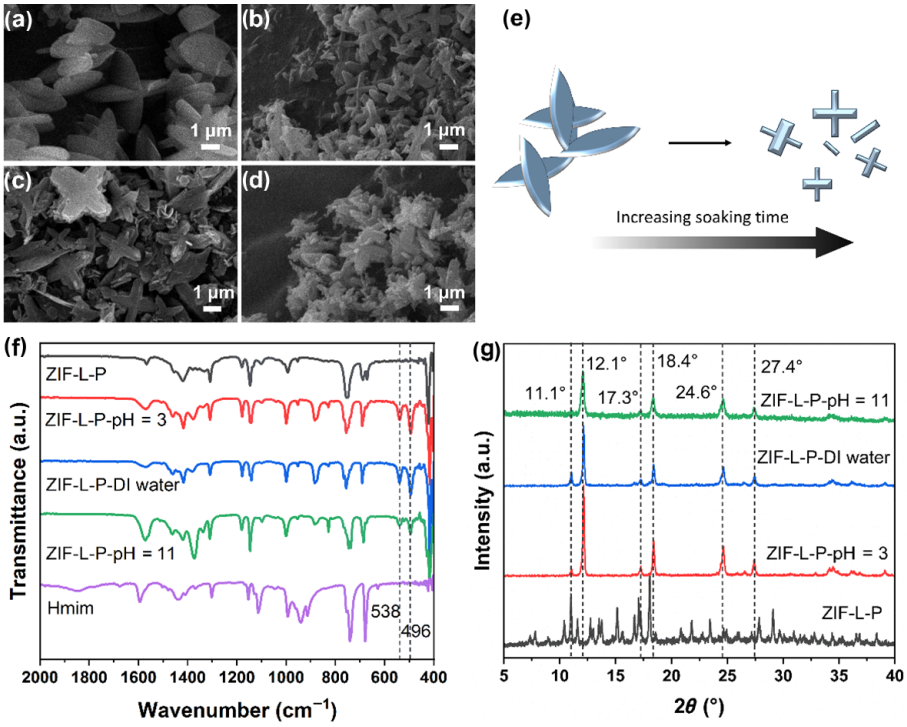

Figure 2 (a) SEM image of ZIF-L crystals. (b)–(d) SEM images of ZIF-L after 24 h in pH = 3 HCl solution, DI water, and pH = 11 NaOH solution, respectively, with a stirring at 1000 rpm. (e) Proposed mechanism for pristine ZIF-L hydrolysis in aqueous media with different pHs. (f) FTIR spectra of Hmim and ZIF-L crystals before and after 24 h in pH = 3 HCl solution, DI water, and pH = 11 NaOH solution. (g) XRD patterns of ZIF-L crystals before and after 24 h in pH = 3 HCl solution, DI water, and pH = 11 NaOH solution.

intensified in the tested samples, especially in the pH = 11 treated sample. The intense and convoluted peaks at 1350–1500 cm^{-1} were associated with the entire ring stretching, and the signal at 1570 cm^{-1} could be assigned as the C=N stretch mode [30]. It was suggested that due to the relatively high pKa value of the Zn–N bond, the hydroxyl group could replace the imidazole during the hydrolysis [32], therefore, more imidazole was kept under basic conditions compared to water and acid.

By comparing the XRD patterns of ZIF-L before and after the stability test, common peaks at 2θ of 11.1° (002), 17.3° (101), and 24.6° (110) were found for both the hydrolysis-tested samples and pristine ZIF-L, which might be contributed by remaining ZIF-L (Fig. 2(g)). New diffraction peaks at 12.1°, 18.4°, and 27.4° were observed in hydrolyzed samples regardless of the pH. The essentially homogenous morphology in Figs. 2(b)–2(d) suggested that the hydrolysis has led to an intermediate crystalline ZIF-type structure. Previous studies of hydrolysis of ZIF materials revealed that dissolution may involve the insertion of a water or acidic molecule into the Zn–N bond, followed by the subsequent dissociation of the protonated imidazole ligand away from the framework structure [17]. It was also suggested that such phase change could be contributed by partly replacing the imidazole molecule with a hydroxyl group and producing a new pseudomorph of ZIF material [32, 34]. Our hydrostability test results agree well with previous studies of powdered ZIF materials. However, in the case of supported ZIF coatings which are packed with ZIF crystals, the hydrolysis mechanism was found different and also not unique due to the limit of water accessibility to different crystal facets, also known as steric hindrance formed by tight ZIF-L packing and intergrowth. These findings provide many new insights which are of practical importance when evaluating the stability of MOF/ZIF coatings and membranes in applications involving humid conditions and aqueous media. Their hydrolysis behaviour may appear completely different from powder samples.

3.2 Enhancement of ZIF-L-SS mesh via protein coating

According to our previous work, pristine ZIF-L coated stainless steel meshes were proved to possess interesting switchable wettability with satisfactory oil/water separation efficiency due to the characteristic leaf-like morphology, thus the morphological change and structural stability in an aqueous environment are of vital importance to its practical application [14]. However, the chemical stability, especially the hydrostability, of ZIF-L meshes appeared to be a huge drawback which significantly hindered their long-term performance. Here, a facile methodology of natural polymer SF protein coating was developed to enhance the stability of ZIF-L-SS meshes in aqueous media. To find the optimum coating recipe for hydrostability improvement of the supported ZIF-L coating, the dissolution process of a series of SF-ZIF-L-SS meshes was systematically studied under various pH conditions.

The primary sequence for the silk fibroin-heavy chain includes larger hydrophilic blocks at the chain ends, six smaller hydrophilic internal blocks, and seven internal hydrophobic blocks, forming hydrophilic–hydrophobic–hydrophilic natural polymers with the capability to form micellar structures in water (Fig. 3(a)) [35, 36]. During the formation of micellar structures in water, the larger terminal hydrophilic blocks define the outer edges of the micelles, while the large hydrophobic blocks and small hydrophilic blocks are present inside the micelles (Fig. 3(a)). The schematic illustration of the protein coating process is shown in Fig. 3(a). With the isoelectric point at ~ 4.2, silk fibroin protein contains a negative surface charge in a neutral aqueous solution due to the acidic charged groups [37]. The negatively charged surface could be connected to the ZIF-L crystals through electrostatic interactions during the coating process. In this work, 3 SF protein concentrations (0.5 wt.%, 1 wt.%, and 3 wt.%) were studied in detail, with the coating time fixed at 1 h. As shown in Figs. 3(b)–3(d), after the coating with 0.5 wt.% and 1 wt.% of SF protein, the edges of the crystals and intracrystalline voids were still relatively clear to observe. However, after being coated with

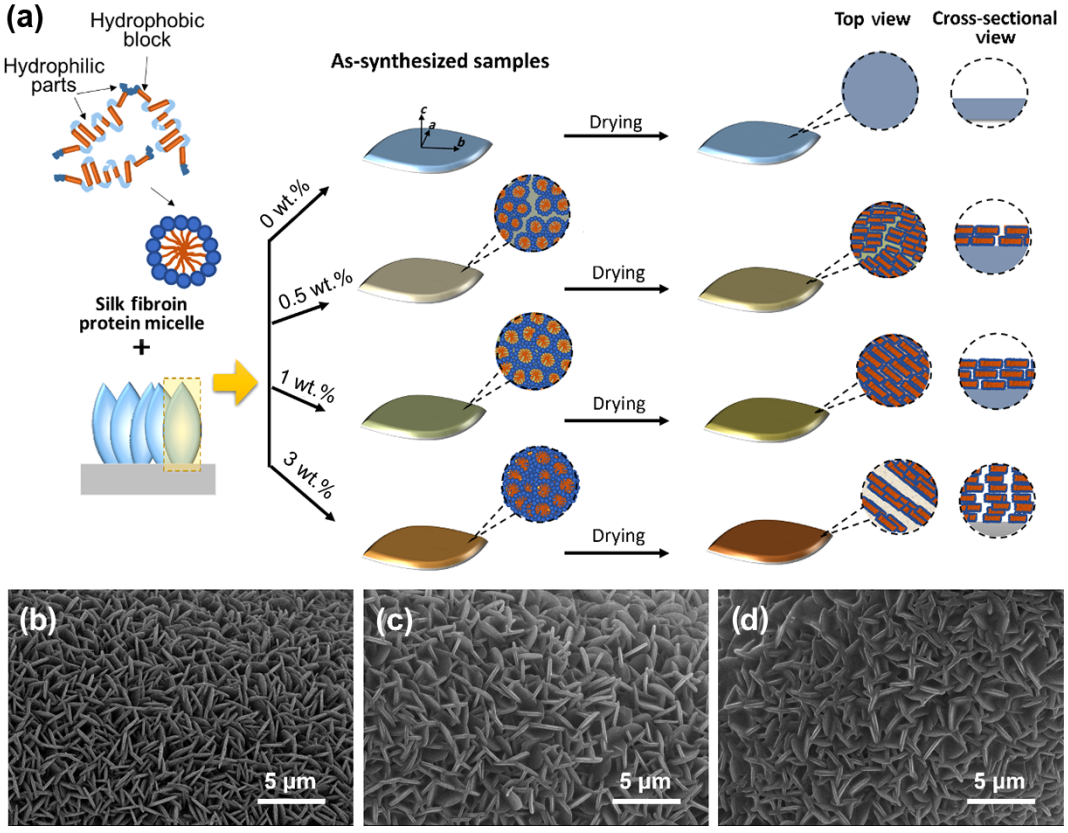

Figure 3 (a) Schematic illustration of the silk fibroin protein ZIF-L mesh coating and drying process. SEM of ZIF-L mesh coated with different protein concentrations (b) 0.5 wt.%, (c) 1 wt.%, and (d) 3 wt.%.

3 wt.% SF protein, as the coating was too thick, the edge of the crystals became smooth, and the surface roughness was reduced. Therefore, SF protein concentrations beyond 3 wt.% were not focused in the following studies.

According to our results (discussed below), a low SF protein concentration of 0.5 wt.% in the coating solution was not enough to form a continuous SF coating on surface ZIF-L crystals. Localized SF coatings exist on the crystal surface and are isolated from each other, forming possible uncovered areas on the crystal (Fig. 1(a)). When the SF protein concentration was increased to 1 wt.%, a more uniform SF coating could be formed, showing a smooth surface with compact SF structures. As also discussed above, a further increase in SF protein concentration to 3 wt.% in our case showed over-coating of the surface crystals, which could lead to many cracks after drying. More details on the structure and stability of surface SF coating were discussed below along with the hydrostability tests of each SF-ZIF-L-SS mesh.

3.2.1 Effect of SF protein coating concentration on the hydrostability of ZIF-L coatings

A series of stability tests were conducted to study the effect of SF coating concentration. As shown in Fig. 3, ZIF-L meshes were first coated with different protein concentrations (0.5 wt.%, 1 wt.%, and 3 wt.%), then soaked in different pH solutions at room temperature. The samples were monitored every 24 h until a significant change in ZIF-L morphology was observed. As shown in Figs. 4(a)–4(c), 0.5 wt.% of SF protein was insufficient to protect the ZIF-L after 3-day soaking in DI water and pH = 3 HCl solution, since most of the surface crystals were broken into smaller pieces and completely fell off from the mesh skeleton after 4 days (see first columns in Figs. S5 and S6 in the ESM). While in pH = 11 NaOH solution, the hierarchical ZIF-L morphology was partly retained after 3 days (Fig. 4(c)) but showed severe damage after 5 days (see first column in Fig. S7 in the ESM).

It is worth noting that no ring etching and unfolding behaviours were observed. Instead, the crystals were broken into small irregularly shaped pieces, which is in good agreement with the proposed localized SF coating structure for 0.5 wt.% SF in Fig. 3(a). The uncoated crystal surface, therefore, appeared to be damaged more easily, leaving random broken pieces falling off from the coating layer. Unfolding of individual crystals was completely inhibited. Overall, even with a low SF coating, the SF-ZIF-L-SS mesh samples showed a significant improvement in the coating hydrostability.

At medium and higher concentrations (1 wt.% and 3 wt.%), SF-ZIF-L-SS meshes were much better protected in pH = 11 NaOH solution compared with those soaked in pH = 3 HCl solution and DI water, as most of the crystals were intact after 3 days of stability test (Figs. 4(d)–4(i)). The stability test results were quite similar in pH = 3 HCl solution and DI water (Figs. S5 and S6 in the ESM). SF-ZIF-L-SS meshes remained intact after 2 days in the aqueous media with a higher concentration of SF protein coating (1 wt.% and 3 wt.%). However, the crystal started to damage after 3 days, and pieces of small ZIF-L crystal residues stayed on the mesh skeleton after 4 days. The stability of SF-ZIF-L-SS mesh in pH = 11 NaOH solution, however, was much better, as shown in Fig. S7 in the ESM. The crystal remained almost intact for the first 4 days with a high concentration of SF coating (1 wt.% and 3 wt.%). Crystals started to show minor damage after 5 days. After 6 or 7 days of soaking, there were still a great number of crystals on the mesh surface. However, the stability performance of 3 wt.% SF protein coating was not significantly better than 1 wt.%.

The SEM results demonstrated the slowest hydrolysis rate of SF-ZIF-L-SS mesh in pH = 11 NaOH solution, and the decomposition in acidic and neutral conditions were comparable. To further understand the crystal dissolution process, Zn^{2+} concentrations that remained in the stability test solution were monitored. For example, SF-ZIF-L-SS meshes coated in the

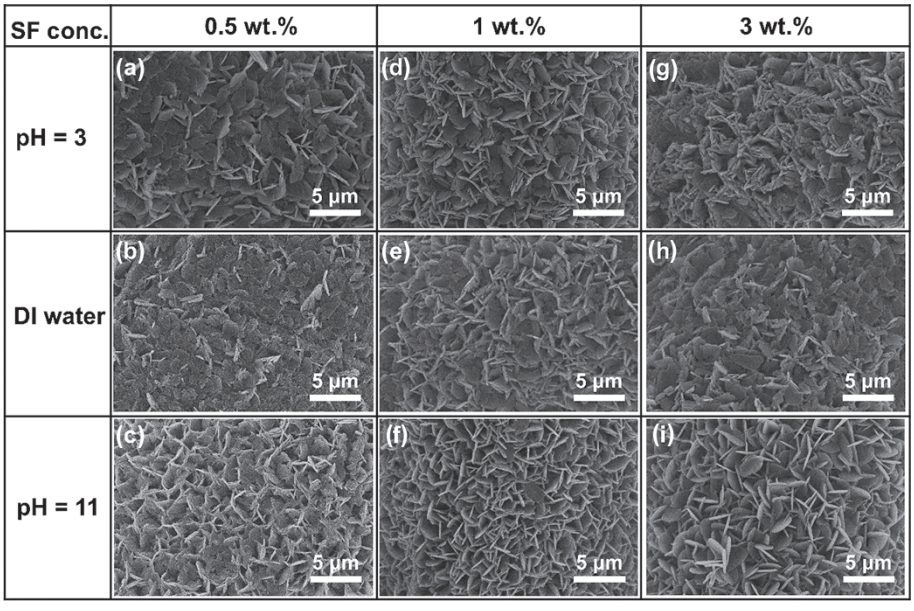

Figure 4 SEM images of SF-ZIF-L-SS meshes after being soaked in aqueous media for 3 days under different pHs.

1 wt.% SF protein were cut to the size of 1 cm × 1.5 cm and soaked in 3 mL of pH = 3 HCl solution, DI water, and pH = 11 NaOH solution. Zn^{2+} concentrations of these solutions were tested after 3 days. According to the inductively coupled plasma (ICP) results (Fig. S8 in the ESM), Zn^{2+} concentration in the testing solutions followed the order of Zn^{2+} (pH = 3) > Zn^{2+} (water) > Zn^{2+} (pH = 11), indicating that the dissolution rate of SF-ZIF-L on the mesh was more significant in acidic condition. A minimum Zn^{2+} concentration of 2.8 mg·L^{-1} was obtained for samples soaked in basic solutions. However, the Zn^{2+} released from the decomposition of ZIF-L in pH = 11 NaOH solution could react with OH^- to form $Zn(OH)_2$ precipitation, which could also lead to the minimal Zn^{2+} in the residue solution. The ICP results together with SEM results indicated that the SF-coated ZIF-L structure was weaker in acidic than in neutral aqueous media, and more stable in basic conditions.

The morphological evolution of each SF-ZIF-L-SS mesh treated under all conditions was summarized and displayed in Fig. 5 for better visualization. 1 wt.% of SF was found to be enough to enhance the ZIF-L coating's hydrostability dramatically.

As discussed above, 0.5 wt.% SF protein was insufficient to protect ZIF-L coatings, and a higher concentration of ≥ 3 wt.% SF also did not prove to be much more promising than 1 wt.% SF coating. To further analyze and understand the SF protein coating effect on individual ZIF-L crystals, ZIF-L powders were coated with 1 wt.% SF protein at the same conditions for further characterization and comparison.

3.2.2 *Effect of SF protein modification on the hydrostability of ZIF-L powders*

To further analyze the effect of SF protein coating, ZIF-L powders were coated with 1 wt.% of SF protein (SF-ZIF-L-P) and tested in aqueous media with various pHs. The FTIR spectra of ZIF-L powders before and after coating are shown in Figs. 6(a) and 6(b).

The enlarged infrared (IR) spectra of the protein-coated sample were dominated by the ZIF-L structure (Fig. 6(b)). The absorption frequencies at ~ 1650 cm^{-1} (amide I), ~ 1530 cm^{-1} (amide II), and ~ 1242 cm^{-1} indicated that the secondary structure of the scaffold is mainly random coli [38]. The morphology of the ZIF-L crystal retained its characteristic leaf-like morphology after protein coating (SEM image in the inset in Fig. 6(b)). The XRD pattern also showed the characteristic ZIF-L structure after 1 wt.% protein coating (Fig. 6(c)). The weak diffraction peak at 2θ = 19.6° (marked by the dashed line) corresponds to silk fibroin protein [39].

Meanwhile, the BET surface area was significantly reduced after protein coating from 116 to 17.39 $m^2 \cdot g^{-1}$. The SF-coated ZIF-L-SS mesh showed a significantly decreased nitrogen adsorption branch compared to that of the pristine ZIF-L sample (Fig. 6(d)). This indicates that the SF coating on ZIF-L crystals has a compact structure which limits the adsorption of nitrogen molecules in the ZIF-L structure.

The SEM images of the hydrolysis of SF-ZIF-L-P in aqueous media are shown in Fig. 7. Most SF-ZIF-L crystals remained intact at the beginning of the stability test (Figs. 7(a)–7(c)), and in the meantime, water molecules and H^+ were penetrating the protein

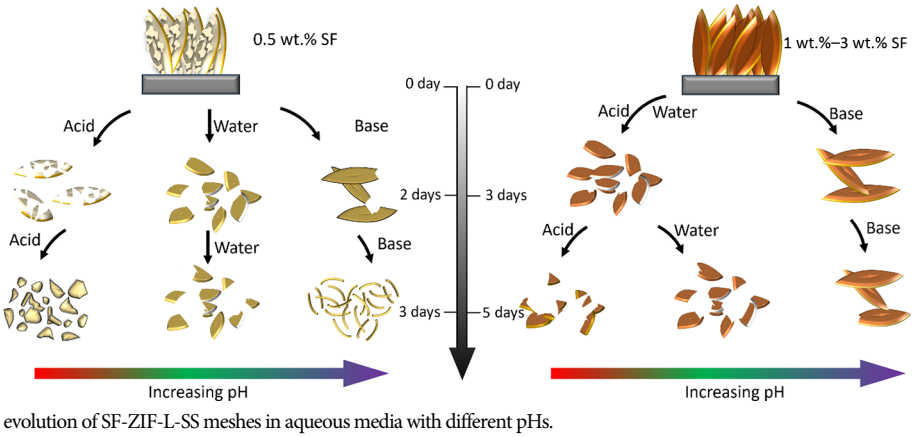

Figure 5 Morphological evolution of SF-ZIF-L-SS meshes in aqueous media with different pHs.

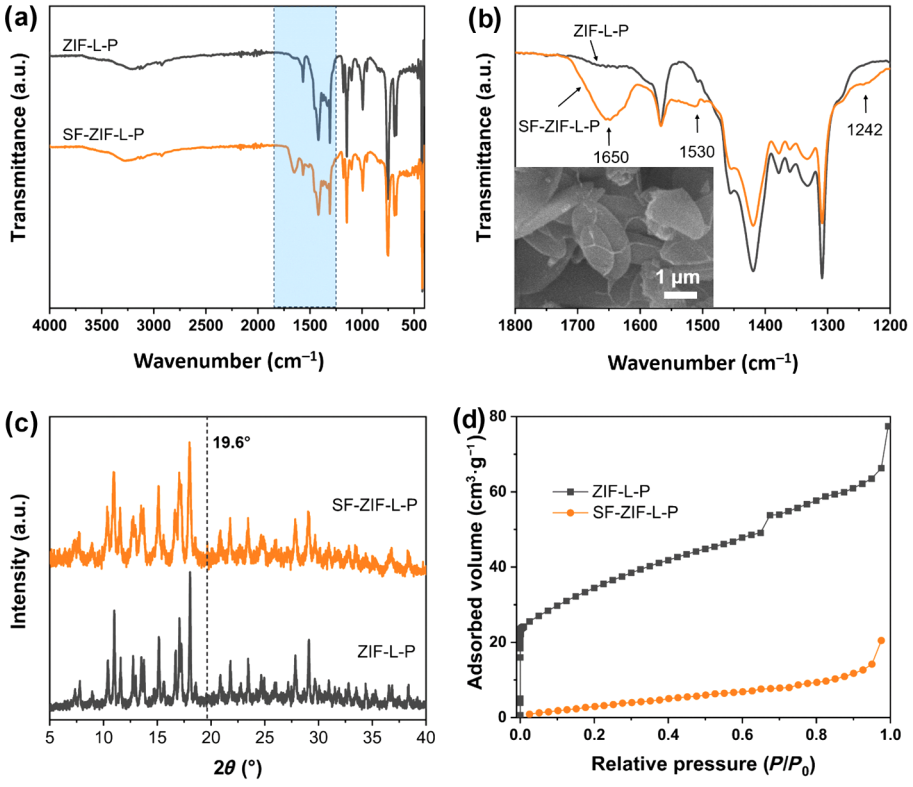

Figure 6 Characterizations of SF-ZIF-L powders. (a) and (b) FTIR spectra of ZIF-L-P with and without 1 wt.% SF protein coating and SEM image of SF-ZIF-L-P (inset). (c) XRD patterns of ZIF-L crystals with and without 1 wt.% SF protein coating. (d) N_2 adsorption plots of ZIF-L-P with and without 1 wt.% SF protein coating.

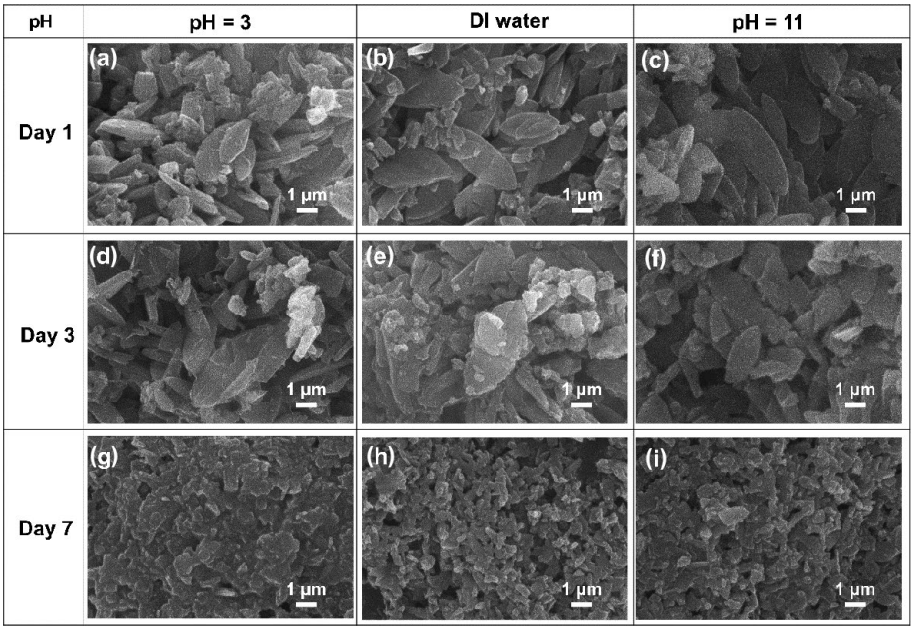

Figure 7 SEM images of 1 wt.% SF protein coated ZIF-L powders after stability test.

layer together with the dissolution of SF protein. With the increase of time to 3 days, these subtle defects on the ZIF-L *ab* plane turned to cracks, therefore crystals broke into pieces (Figs. 7(d)–7(f)). After 7 days, these crystals became smaller, and then fully decomposed (Figs. 7(g)–7(i)).

The schematic illustration of ZIF-L hydrolysis is shown in Fig. 8(a). The SF-ZIF-L crystals remained intact at the beginning of the stability test, and in the meantime, water molecules and H^+ were penetrating the protein layer together with the dissolution of SF protein. With the increase of time, SF-ZIF-L crystals broke into pieces. Afterwards, these crystals pieces became smaller, and then fully decomposed. The FTIR spectra of protein-coated ZIF-L before and after the stability test are shown in Figs. 8(b) and 8(c). After 3 days of treatment, its IR spectrum was still dominated by ZIF-L, and the characteristic signals of hydrolyzed uncoated ZIF-L powders at ~ 494 and ~ 539 cm^{-1} were observed, which indicated the hydrolysis of SF-ZIF-L-P. Meanwhile, the peaks at ~ 1625, ~ 1530, and ~ 1235 cm^{-1} were observed on the spectra of SF-ZIF-L-P samples after the 3-day stability test, reflecting a transition of random coil conformation to β-sheet (silk II) during the hydrolysis test [40], which is a more stable structure of SF protein [37]. Leaf-like ZIF-L crystals and amorphous ZIF-L residues were observed in the SEM image, further confirming that SF-ZIF-L-P was partly hydrolyzed in the stability test (Figs. 7(d)–7(f)).

XRD patterns of the pristine and soaked SF protein-coated ZIF-L samples are shown in Fig. 8(d) with all of them showing intact

characteristic ZIF-L diffraction peaks. Furthermore, the previously observed peaks at 2θ = 12.14°, 18.4°, and 24.6° of the hydrolyzed intermediate ZIF structure found on soaked SF-ZIF-L-SS meshes were not present anymore, indicating that the hydrolysis of ZIF-L crystals was significantly reduced with the protein coating as compared with uncoated ZIF-L powder. The diffraction peak at 2θ = 19.6° corresponding to SF protein structure could not be found in Fig. 8(e), indicating the partial dissolution of SF protein during the stability tests. The BET surface area of the sample after the stability test in pH = 3 HCl solution increased a little to 22.83 $m^2 \cdot g^{-1}$ (Fig. 8(e)), which strongly confirmed the protective function of the dense SF protein coating and negligible decomposition of the protein structure under such acidic conditions. Nitrogen adsorption of these 2 samples showed quite similar adsorption branches, further suggesting a similar SF-ZIF-L structure before and after the hydrostability test.

3.3 Oil/water separation performance of silk fibroin-coated ZIF-L meshes

The stability of ZIF materials in acidic and basic environments is of major concern [13]. As discussed above, SF-ZIF-L-SS mesh exhibited enhanced stability with well-retained surface morphology. In this section, the wetting property and oil/water separation performance were further monitored to test the application of SF-ZIF-L-SS meshes.

3.3.1 Surface wettability of protein-coated ZIF-L meshes

The surface wetting property of the ZIF-L meshes after protein coating was characterized by water contact angle (WCA) measurement (Figs. 9(a)–9(f) and Fig. S9 in the ESM). The wettability of ZIF-L-SS, SF-ZIF-L-SS, and SF-ZIF-L-SS-pH3 meshes (SF-ZIF-L-SS mesh after 3 days in pH = 3 HCl solution) was all hydrophilic with WCAs of ~ 35.1°, ~ 37.2°, and ~ 35.5°, respectively (Fig. S9 in the ESM). The switchable wetting properties of ZIF-L-SS meshes were monitored by underwater oil contact angle and underoil water contact angle. The underwater wettability of ZIF-L-SS, SF-ZIF-L-SS, and SF-ZIF-L-SS-pH3 meshes were explored by immersing the mesh in water and performing oil (chloroform) contact angle measurements. The underwater oil contact angles of ZIF-L-SS, SF-ZIF-L-SS, and SF-ZIF-L-SS-pH3 meshes were ~ 155°, ~ 160°, and ~ 161°, respectively, suggesting that the outstanding underwater superoleophobicity was unchanged after the SF protein coating and stability test in an acidic environment. The underoil wettability of ZIF-L-SS, SF-ZIF-L-SS, and SF-ZIF-L-SS-pH3 meshes was also examined by immersing the mesh in oil (hexane) and performing water contact angle measurements. ZIF-L-SS, SF-ZIF-L-SS, and SF-ZIF-L-SS-pH3 meshes exhibited underoil superhydrophobicity with underoil water contact angles of ~ 162°, ~ 161°, and ~ 151°, respectively. It was therefore suggested that the switchable wetting property was retained after SF protein coating, and even after the stability of the SF-ZIF-L-SS mesh in an acidic environment.

3.3.2 Oil/water separation performance

Gravity-driven oil/water separation tests were carried out because

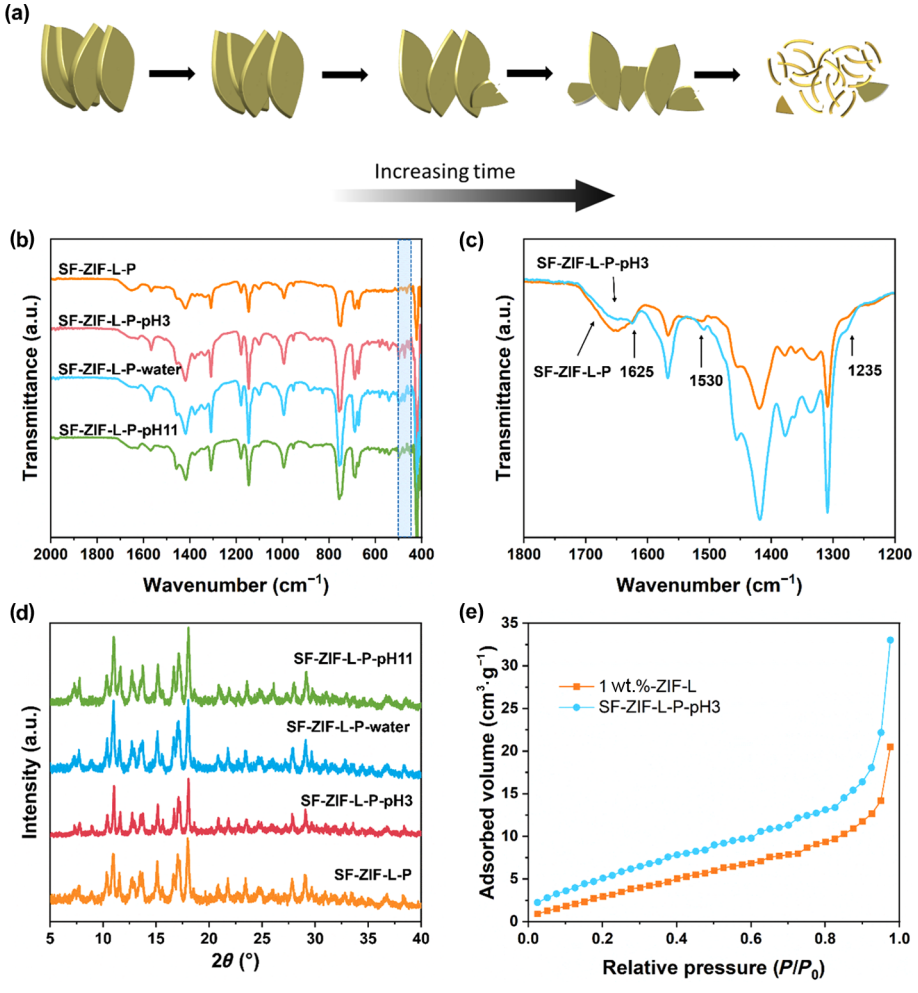

Figure 8 (a) Schematic illustration of SF-ZIF-L-P hydrolysis. (b) and (c) FTIR spectra of SF-ZIF-L-P before and after 3 days in pH = 3 HCl solution, DI water, and pH = 11 NaOH solution, respectively. (d) XRD patterns of 1 wt.% protein coated SF-ZIF-L-P before and after 3 days in pH = 3 HCl solution, DI water, and pH = 11 NaOH solution. (e) N_2 gas adsorption slot of 1 wt.% protein coated ZIF-L before and after 3 days in pH = 3 HCl solution.

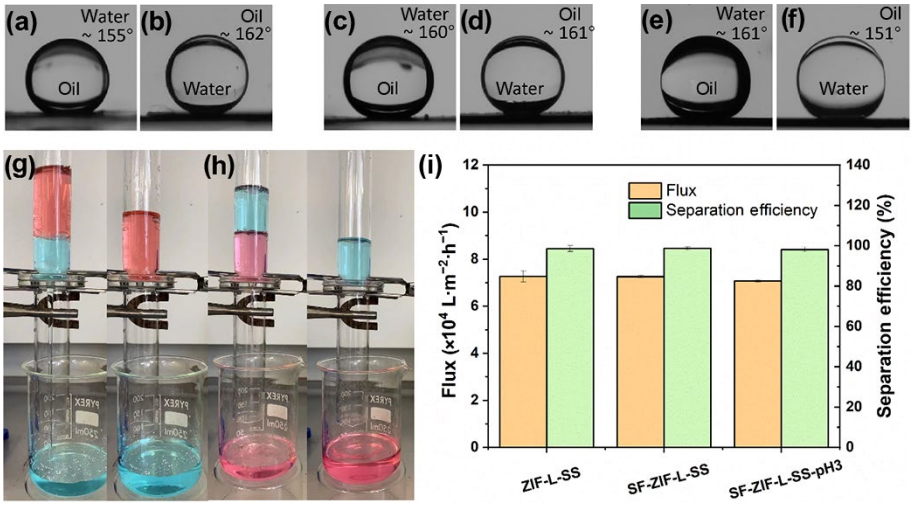

Figure 9 Photographs of underwater oil contact angles and underoil water contact angles of (a) and (b)ZIF-L mesh, (c) and (d) SF-ZIF-L-SS mesh, and (e) and (f) SF-ZIF-L-SS mesh after 3 days in pH = 3 HCl solution. (g) Photographs of water pre-wetted oil-blocking separation. (h) Photographs of oil pre-wetted water-blocking separatio. (i) Flux and separation efficiency of ZIF-L-SS mesh, SF-ZIF-L-SS mesh, and SF-ZIF-L-SS mesh after 3 days in pH = 3 HCl solution.

the superior superwetting properties of ZIF-L coated mesh films allowed the separation driven solely by gravity. The ZIF-L-SS mesh was confirmed with switchable oil/water separation ability in the previous section. When pre-wetted with water, the water molecules preferentially permeated through the mesh while the oil molecules were rejected because of their underwater superoleophobicity. On the contrary, when prewetted with oil, ZIF-L mesh film preferentially lets oil go through while rejecting water due to underoil superhydrophobicity [14].

The switchable oil/water separation tests are shown in Figs. 9(g) and 9(h). Firstly, a mixture of oil red-dyed cyclohexane and methylene blue-dyed water ($\rho_{water} > \rho_{oil}$) was poured onto the water-prewetted mesh, triggering "oil-blocking" separation, as cyclohexane was rejected above the mesh surface despite being in contact with the surface at the beginning. After cleaned with ethanol and air drying, the mesh was then prewetted with chloroform. Then, a mixture of water and chloroform ($\rho_{oil} > \rho_{water}$) was poured into a funnel. It was observed that only chloroform permeated through the mesh while the water was completely blocked, confirming that the separation was successfully switched to the "water-blocking" separation mode. All the separation processes were solely driven by gravity, and no external pressure was applied. As shown in Fig. 9(i), the separation efficiencies of ZIF-L-SS mesh with and without protein coating for n-heptane were above 98% with a permeate flux of ~ 7.2×10^4 L·m^{-2}·h^{-1}, suggesting that the mesh preserved its switchable oil/water separation property after the protein coating. The results demonstrated comparable separation efficiency and flux to those reported in other studies [41]. Furthermore, the oil/water separation performance of SF-ZIF-L-SS mesh after the stability test in pH3 solution was also measured. The SF-ZIF-L-SS-pH3 mesh showed an oil/water separation efficiency of over 98% and a flux of over 7.0×10^4 L·m^{-2}·h^{-1}, suggesting that the satisfactory oil/water separation property was retained after the acidic stability test.

4 Conclusions

In this work, the hydrolysis of supported ZIF-L coatings and powders was systematically studied under different pHs. Interestingly, the etching and unfolding behaviour of ZIF-L coatings were observed in aqueous media regardless of the pH. Natural polymer SF protein coating was used to modify the ZIF-L crystal surface and proved to be effective for the enhancement of the hydrostability of both ZIF-L coatings and powder samples in aqueous media. The characteristic leaf-like morphology of ZIF-L on the mesh was retained for up to 3 days in water and acid and 5 days in basic solution. The SF-ZIF-L-SS meshes preserved their switchable superwetting properties with superior separation performance for oil/water mixture separation with a permeation flux as high as ~ 7×10^4 L·m^{-2}·h^{-1} and an oil removal efficiency of above 98%.

Acknowledgements

This work was supported by start-up funding from the School of Engineering, at the University of Edinburgh. X. M. W. thanks the University of Edinburgh for Principal's Career Development Ph.D. Scholarships and the School of Engineering for Edinburgh Global Research Scholarship. The authors would like to thank Fergus Dingwall for his laboratory assistance.

Electronic Supplementary Material: Supplementary material (further details of the stability tests of ZIF-L-SS meshes at varied aqueous conditions, SEM imaging, and water contact angles) is available in the online version of this article at https://doi.org/10.1007/s12274-024-6586-5.

References

[1] Zhou, H. C. J.; Kitagawa, S. Metal-organic frameworks (MOFs). *Chem. Soc. Rev.* **2014**, *43*, 5415–5418.

[2] Seetharaj, R.; Vandana, P. V.; Arya, P.; Mathew, S. Dependence of solvents, pH, molar ratio and temperature in tuning metal-organic

framework architecture. *Arab. J. Chem.* **2019**, *12*, 295–315.
[3] Pan, Y. C.; Liu, Y. Y.; Zeng, G. F.; Zhao, L.; Lai, Z. P. Rapid synthesis of zeolitic imidazolate framework-8 (ZIF-8) nanocrystals in an aqueous system. *Chem. Commun.* **2011**, *47*, 2071–2073.
[4] Cacho-Bailo, F.; Seoane, B.; Téllez, C.; Coronas, J. ZIF-8 continuous membrane on porous polysulfone for hydrogen separation. *J. Memb. Sci.* **2014**, *464*, 119–126.
[5] Lei, Z. W.; Deng, Y. H.; Wang, C. Y. Multiphase surface growth of hydrophobic ZIF-8 on melamine sponge for excellent oil/water separation and effective catalysis in a Knoevenagel reaction. *J. Mater. Chem. A* **2018**, *6*, 3258–3263.
[6] Zheng, H. Q.; Zhang, Y. N.; Liu, L. F.; Wan, W.; Guo, P.; Nyström, A. M.; Zou, X. D. One-pot synthesis of metal-organic frameworks with encapsulated target molecules and their applications for controlled drug delivery. *J. Am. Chem. Soc.* **2016**, *138*, 962–968.
[7] Xiao, H.; Zhou, H. X.; Feng, S. S.; Gore, D. B.; Zhong, Z. X.; Xing, W. H. *In situ* growth of two-dimensional ZIF-L nanoflakes on ceramic membrane for efficient removal of iodine. *J. Memb. Sci.* **2021**, *619*, 118782.
[8] Yuan, S. S.; Zhu, J. Y.; Li, Y.; Zhao, Y.; Li, J.; Van Puyvelde, P.; Van Der Bruggen, B. Structure architecture of micro/nanoscale ZIF-L on a 3D printed membrane for a superhydrophobic and underwater superoleophobic surface. *J. Mater. Chem. A* **2019**, *7*, 2723–2729.
[9] Ding, M. L.; Cai, X. C.; Jiang, H. L. Improving MOF stability: Approaches and applications. *Chem. Sci.* **2019**, *10*, 10209–10230.
[10] Leus, K.; Bogaerts, T.; De Decker, J.; Depauw, H.; Hendrickx, K.; Vrielinck, H.; Van Speybroeck, V.; Van Der Voort, P. Systematic study of the chemical and hydrothermal stability of selected "stable" metal-organic frameworks. *Microporous Mesoporous Mater.* **2016**, *226*, 110–116.
[11] Park, K. S.; Ni, Z.; Côté, A. P.; Choi, J. Y.; Huang, R. D.; Uribe-Romo, F. J.; Chae, H. K.; O'Keeffe, M.; Yaghi, O. M. Exceptional chemical and thermal stability of zeolitic imidazolate frameworks. *Proc. Natl. Acad. Sci. USA* **2006**, *103*, 10186–10191.
[12] Bhattacharyya, S.; Pang, S. H.; Dutzer, M. R.; Lively, R. P.; Walton, K. S.; Sholl, D. S.; Nair, S. Interactions of SO_2-containing acid gases with ZIF-8: Structural changes and mechanistic investigations. *J. Phys. Chem. C* **2016**, *120*, 27221–27229.
[13] Mottillo, C.; Friščić, T. Carbon dioxide sensitivity of zeolitic imidazolate frameworks. *Angew. Chem., Int. Ed.* **2014**, *53*, 7471–7474.
[14] Chen, T.; Lewis, A.; Chen, Z. P.; Fan, X. F.; Radacsi, N.; Semiao, A. J. C.; Wang, H. T.; Huang, Y. Smart ZIF-L mesh films with switchable superwettability synthesized via a rapid energy-saving process. *Sep. Purif. Technol.* **2020**, *240*, 116647.
[15] Yuan, S.; Feng, L.; Wang, K. C.; Pang, J. D.; Bosch, M.; Lollar, C.; Sun, Y. J.; Qin, J. S.; Yang, X. Y.; Zhang, P. et al. Stable metal-organic frameworks: Design, synthesis, and applications. *Adv. Mater.* **2018**, *30*, 1704303.
[16] Qadir, N. U.; Said, S. A. M.; Bahaidarah, H. M. Structural stability of metal-organic frameworks in aqueous media—Controlling factors and methods to improve hydrostability and hydrothermal cyclic stability. *Microporous Mesoporous Mater.* **2015**, *201*, 61–90.
[17] Gao, S.; Hou, J. W.; Deng, Z. Y.; Wang, T. S.; Beyer, S.; Buzanich, A. G.; Richardson, J. J.; Rawal, A.; Seidel, R.; Zulkifli, M. Y. et al. Improving the acidic stability of zeolitic imidazolate frameworks by biofunctional molecules. *Chem* **2019**, *5*, 1597–1608.
[18] Liu, X. L.; Li, Y. S.; Ban, Y. J.; Peng, Y.; Jin, H.; Bux, H.; Xu, L. Y.; Caro, J.; Yang, W. S. Improvement of hydrothermal stability of zeolitic imidazolate frameworks. *Chem. Commun.* **2013**, *49*, 9140–9142.
[19] Shih, Y. H.; Kuo, Y. C.; Lirio, S.; Wang, K. Y.; Lin, C. H.; Huang, H. Y. A simple approach to enhance the water stability of a metal-organic framework. *Chem.—Eur. J.* **2017**, *23*, 42–46.
[20] Zu, D. D.; Lu, L.; Liu, X. Q.; Zhang, D. Y.; Sun, L. B. Improving hydrothermal stability and catalytic activity of metal-organic frameworks by graphite oxide incorporation. *J. Phys. Chem. C* **2014**, *118*, 19910–19917.
[21] Yang, S. J.; Choi, J. Y.; Chae, H. K.; Cho, J. H.; Nahm, K. S.; Park, C. R. Preparation and enhanced hydrostability and hydrogen storage capacity of CNT@MOF-5 hybrid composite. *Chem. Mater.* **2009**, *21*, 1893–1897.
[22] Zhang, W.; Hu, Y. L.; Ge, J.; Jiang, H. L.; Yu, S. H. A facile and general coating approach to moisture/water-resistant metal-organic frameworks with intact porosity. *J. Am. Chem. Soc.* **2014**, *136*, 16978–16981.
[23] Zhang, F.; You, X. R.; Dou, H.; Liu, Z.; Zuo, B. Q.; Zhang, X. G. Facile fabrication of robust silk nanofibril films via direct dissolution of silk in $CaCl_2$-formic acid solution. *ACS Appl. Mater. Interfaces* **2015**, *7*, 3352–3361.
[24] Wang, X. Q.; Yucel, T.; Lu, Q.; Hu, X.; Kaplan, D. L. Silk nanospheres and microspheres from silk/PVA blend films for drug delivery. *Biomaterials* **2010**, *31*, 1025–1035.
[25] Jin, H. J.; Kaplan, D. L. Mechanism of silk processing in insects and spiders. *Nature* **2003**, *424*, 1057–1061.
[26] Zhang, L.; Hu, Y. H. Strong effects of higher-valent cations on the structure of the zeolitic Zn(2-methylimidazole)$_2$ framework (ZIF-8). *J. Phys. Chem. C* **2011**, *115*, 7967–7971.
[27] Lee, S.; Oh, S.; Oh, M. Atypical hybrid metal-organic frameworks (MOFs): A combinative process for MOF-on-MOF growth, etching, and structure transformation. *Angew. Chem., Int. Ed.* **2020**, *59*, 1327–1333.
[28] Chen, R. Z.; Yao, J. F.; Gu, Q. F.; Smeets, S.; Baerlocher, C.; Gu, H. X.; Zhu, D. R.; Morris, W.; Yaghi, O. M.; Wang, H. T. A two-dimensional zeolitic imidazolate framework with a cushion-shaped cavity for CO_2 adsorption. *Chem. Commun.* **2013**, *49*, 9500–9502.
[29] Low, Z. X.; Yao, J. F.; Liu, Q.; He, M.; Wang, Z. Y.; Suresh, A. K.; Bellare, J.; Wang, H. T. Crystal transformation in zeolitic-imidazolate framework. *Cryst. Growth Des.* **2014**, *14*, 6589–6598.
[30] Ding, B.; Wang, X. B.; Xu, Y. F.; Feng, S. J.; Ding, Y.; Pan, Y.; Xu, W. F.; Wang, H. T. Hydrothermal preparation of hierarchical ZIF-L nanostructures for enhanced CO_2 capture. *J. Colloid Interface Sci.* **2018**, *519*, 38–43.
[31] Lo, Y.; Lam, C. H.; Chang, C. W.; Yang, A. C.; Kang, D. Y. Polymorphism/pseudopolymorphism of metal-organic frameworks composed of zinc(II) and 2-methylimidazole: Synthesis, stability, and application in gas storage. *RSC Adv.* **2016**, *6*, 89148–89156.
[32] Zhang, H. F.; Zhao, M.; Yang, Y.; Lin, Y. S. Hydrolysis and condensation of ZIF-8 in water. *Microporous Mesoporous Mater.* **2019**, *288*, 109568.
[33] Hu, Y.; Kazemian, H.; Rohani, S.; Huang, Y. N.; Song, Y. *In situ* high pressure study of ZIF-8 by FTIR spectroscopy. *Chem. Commun.* **2011**, *47*, 12694–12696.
[34] Zhang, H. F.; Zhao, M.; Lin, Y. S. Stability of ZIF-8 in water under ambient conditions. *Microporous Mesoporous Mater.* **2019**, *279*, 201–210.
[35] Mita, K.; Ichimura, S.; James, T. C. Highly repetitive structure and its organization of the silk fibroin gene. *J. Mol. Evol.* **1994**, *38*, 583–592.
[36] Zhou, C. Z.; Confalonieri, F.; Medina, N.; Zivanovic, Y.; Esnault, C.; Yang, T.; Jacquet, M.; Janin, J.; Duguet, M.; Perasso, R. et al. Fine organization of *Bombyx mori* fibroin heavy chain gene. *Nucleic Acids Res.* **2000**, *28*, 2413–2419.
[37] Lu, Q.; Zhu, H. S.; Zhang, C. C.; Zhang, F.; Zhang, B.; Kaplan, D. L. Silk self-assembly mechanisms and control from thermodynamics to kinetics. *Biomacromolecules* **2012**, *13*, 826–832.
[38] Hu, Y.; Zhang, Q.; You, R.; Wang, L.; Li, M. The relationship between secondary structure and biodegradation behavior of silk fibroin scaffolds. *Adv. Mater. Sci. Eng.* **2012**, *2012*,
[39] Kundu, J.; Chung, Y. I.; Kim, Y. H.; Tae, G.; Kundu, S. C. Silk fibroin nanoparticles for cellular uptake and control release. *Int. J. Pharm.* **2010**, *388*, 242–250.
[40] Zhang, Y. Q.; Shen, W. D.; Xiang, R. L.; Zhuge, L. J.; Gao, W. J.; Wang, W. B. Formation of silk fibroin nanoparticles in water-miscible organic solvent and their characterization. *J. Nanopart. Res.* **2007**, *9*, 885–900.
[41] Li, Q. Q.; Deng, W. J.; Li, C. H.; Sun, Q. Y.; Huang, F. Z.; Zhao, Y.; Li, S. K. High-flux oil/water separation with interfacial capillary effect in switchable superwetting Cu(OH)$_2$@ZIF-8 nanowire membranes. *ACS Appl. Mater. Interfaces* **2018**, *10*, 40265–40273.